https://doi.org/10.1016/j.powtec.2022.118163

Highlights

Particle resuspension from a flow-induced fluttering flexible substrate

Jie Feng [a], Cunteng Wang [a], Yi Zhang [a], Ka Chung Chan [a], Chun Ho Liu [a], Christopher Y.H. Chao [b, c], Sau Chung Fu [b, *]

[a] Department of Mechanical Engineering, The University of Hong Kong, Hong Kong, China

[b] Department of Building Environment and Energy Engineering, The Hong Kong Polytechnic University, Hong Kong, China

[c] Department of Mechanical Engineering, The Hong Kong Polytechnic University, Hong Kong, China

[*] Corresponding author. E-mail address: schung.fu@polyu.edu.hk (S.C. Fu).

- Fluttering substrate and particle resuspension were quantified and correlated.
- A fluttering substrate enhanced particle resuspension compared with the fixed one.
- Particle diameter and position were observed to influence particle resuspension.
- A force caused by fluttering acceleration was identified as an important factor.
- An aerodynamic force/moment enhancement was another necessary factor.

Abstract

Particle resuspension from a flow-induced fluttering flexible substrate

Jie Feng [a], Cunteng Wang [a], Yi Zhang [a], Ka Chung Chan [a], Chun Ho Liu [a], Christopher Y.H. Chao [b, c], Sau Chung Fu [b, *]

[a] Department of Mechanical Engineering, The University of Hong Kong, Hong Kong, China

[b] Department of Building Environment and Energy Engineering, The Hong Kong Polytechnic University, Hong Kong, China

[c] Department of Mechanical Engineering, The Hong Kong Polytechnic University, Hong Kong, China

[*] Corresponding author. E-mail address: schung.fu@polyu.edu.hk (S.C. Fu).

ABSTRACT

Resuspension of spherical particles from a flow-induced fluttering, partially free, flexible substrate was experimentally studied. The effects of the flow-induced flutter on the particle resuspension, and the underlying mechanisms initiating the particle resuspension in the fluttering substrate case, were quantitatively illustrated by comparing with the fixed substrate case. The results show that the flow-induced flutter of the substrate remarkably enhanced the particle resuspension and greatly reduced the threshold velocity. A force caused by the fluttering acceleration of the substrate was identified as an important factor enhancing the particle resuspension. The existence of a significant flutter-induced aerodynamic force/moment enhancement acting on the particles was demonstrated, and it was another necessary factor promoting the particle resuspension. This paper not only reveals the phenomenon of particle resuspension by the flow-induced flutter of the flexible substrate, but also provides useful information for facilitating or preventing the particle resuspension in the industrial and environmental fields.

Keywords: Particle; Resuspension; Airflow; Flutter; Flexible substrate.

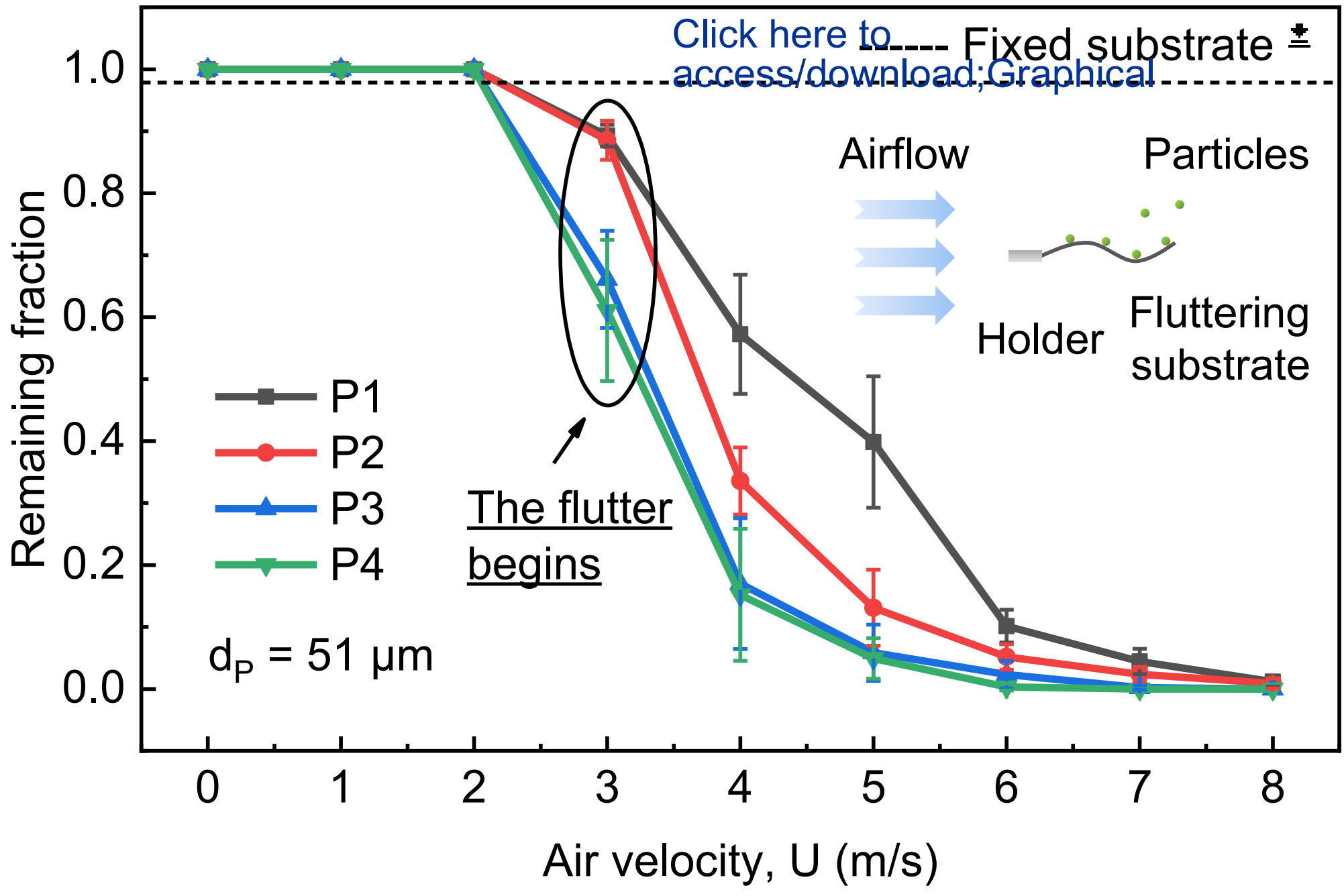
Click here to access/download;Graphical
Fixed substrate
Airflow
Particles
Holder
Fluttering substrate
P1
P2
P3
P4
The flutter begins
d_P = 51 μm
Remaining fraction
Air velocity, U (m/s)
0.0
0.2
0.4
0.6
0.8
1.0
0
1
2
3
4
5
6
7
8

Manuscript

Particle resuspension from a flow-induced fluttering flexible substrate

Jie Feng [a], Cunteng Wang [a], Yi Zhang [a], Ka Chung Chan [a], Chun Ho Liu [a], Christopher Y.H. Chao [b, c], Sau Chung Fu [b, *]

[a] Department of Mechanical Engineering, The University of Hong Kong, Hong Kong, China

[b] Department of Building Environment and Energy Engineering, The Hong Kong Polytechnic University, Hong Kong, China

[c] Department of Mechanical Engineering, The Hong Kong Polytechnic University, Hong Kong, China

[*] Corresponding author. E-mail address: schung.fu@polyu.edu.hk (S.C. Fu).

1. Introduction

Particle resuspension, a phenomenon in which particles originally deposited on a surface are detached from and transported away from the surface, has been extensively studied in a wide range of industrial and environmental fields [1]. Understanding the behavior of particle resuspension contributes to facilitating industrial manufacturing operations and building healthy living environments [2-4].

Over the past few decades, extensive experimental work has been carried out on particle resuspension from flat surfaces under the influence of airflow [5-10]. Wu et al. [5] systematically investigated the effects of air velocity, particle size/type, and relative humidity on particle resuspension in wind tunnel experiments by optical microscopy-video camera techniques. Ibrahim et al. [6] reported the detachment modes of microparticles adhering to flat surfaces exposed to turbulent airflow. Jiang et al. [7] explored the effect of surface roughness on particle-surface interaction by the airflow method, and Kim et al. [9] conducted wind tunnel experiments to evaluate the effect of relative humidity on the resuspension rates of different particle-surface combinations. A planar Particle Image Velocimetry system was employed to characterize particle-fluid interaction by Barth et al. [8], and particle-particle interaction before the flow-induced resuspension was recognized by Rondeau et al. [10] according to theory as well as wind tunnel experimental results.

A number of models describing the flow-induced particle resuspension from flat surfaces have also been developed [11-19]. Ziskind et al. [11] described particle resuspension on the basis of force/moment balance. Likewise, Reeks and Hall [12] developed an energy-accumulation model elucidating the drag and lift forces in particle resuspension. Tran-Cong et al. [13] and Fillingham et al. [14] formulated a set of correlations for predicting the lift and drag coefficients affecting the aerodynamic forces. Monte Carlo

simulations have been utilized for developing particle resuspension models accounting for the effects of surface roughness, adhesive force distribution, turbulent burst, and particle shape [15-18]. Nasr et al. [19] presented a rolling detachment model for particles residing on flat surfaces with large-scale roughness in a turbulent flow. Therefore, the fundamental mechanisms of particle resuspension have been fostered. For the flow-induced resuspension of a single particle, there are three possible modes governing its incipient motion on a flat surface: lift-off, sliding and rolling, when the static equilibrium of the particle on the surface is no longer fulfilled. For example, from the perspective of a force/moment balance, the resuspension can be interpreted simply as a competition between removal and adhesive forces/moments acting on the particle. In other words, the processes of lift-off and sliding can be explained by the force unbalance, while the rolling process can be illustrated in terms of rupturing the moment balance around the rolling point.

In addition to the flow-induced resuspension, vibration of a contaminated surface excited by external forces can cause particle resuspension [20]. Hein et al. [21] and Hubbard et al. [22] demonstrated the effectiveness of wafer substrate vibration in resuspending the deposited particles and correlated the substrate acceleration with the particle dynamics. Chatoutsidou and Lazaridis [23] investigated the resuspension of spherical particles from a glass plate subjected to an external vibrating force. It was found that a slight deformation in the body of the plate occurred and propagated via bending waves. When the surface is flexible, the deformation is greater. Wang et al. [24] pointed out that the deformation of a cloth surface together with the resulting turbulent airflow and particle agglomeration were contributing factors to the particle detachment, when the cloth was subjected to a rod strike.

In the absence of these external excitations, a flexible surface would also vibrate and deform (i.e., flutter) when it is exposed to an airflow, due to the excitation of a resonant bending instability [25]. In fact, such flow-induced flutter is a common motion mode of flexible surfaces, such as a flag fluttering in the wind. The wind velocity has been recognized as an important parameter related to the fluttering dynamics of flags [26]. In this case, the airflow and surface motion may work together to resuspend the particles, indicating that this phenomenon could further refine the above-mentioned theoretical models. Although the flutter phenomenon has been widely investigated in many fields, including fluid dynamics [26], energy harvesting [27] and heat transfer [28], it is rarely discussed in the context of particle resuspension. While studying particle deposition on plant leaves, Giess et al. [29], Petroff et al. [30] and Zhang et al. [31] found that leaf flutter was an undesired phenomenon that could promote resuspension. On the other hand, the flow-

induced flutter was considered advantageous to de-aggregate and aerosolize drugs for dry powder inhalers (DPIs) [32, 33]. The fluttering polymer films were used to optimize the drug dispersion from the films. The flutter phenomenon deserves more attention in our field as a potential approach to aerosolize particles, but the underlying mechanisms of particle resuspension from a fluttering substrate have yet to be clarified.

To help fill this knowledge gap, an experimental study on particle resuspension from a flow-induced fluttering flexible substrate is presented in this paper. The substrate fluttering dynamics and the resuspension behavior of monolayer particles were both examined by investigating some key parameters including air velocity, fluttering frequency and acceleration of the substrate, particle size, position on the substrate, remaining fraction of particles on the substrate, and forces/moments acting on a particle. Moreover, a control experiment of fixing the substrate was carried out under the same conditions. By comparing with the fixed substrate case, the effects of the fluttering dynamics on particle resuspension, and the underlying mechanisms initiating particle resuspension in the fluttering substrate case, were quantitatively explored.

2. Materials and methods

Polystyrene (PS) spherical particles with a density of 1.05 g/cm^3 and four diameters of 6 μm, 13 μm, 31 μm, and 51 μm were used as the test particles in the present work. The coefficients of variation (CV%) for the four particle sizes were 12%, 14%, 9%, and 12% respectively. The flexible substrate was a 0.023-mm-thick transparent plastic film made of oriented polypropylene (OPP). The surface energy of these materials was determined using testing liquids (Test Inks, Arcotest, Germany), and the Young's modulus was measured by a nanoindenter (NanoTest Vantage, Micro Materials, UK). The material properties are summarized in Table 1.

Table 1

The particle resuspension experiments were performed in a subsonic wind tunnel (C2, Armfield, UK) at an ambient temperature of 26.8 ± 0.3 ℃, a relative humidity of 67 ± 2%, and air velocities of 0 ~ 8 m/s (Figure 1a). In order to avoid particle aging biasing the resuspension results, the experiments were conducted immediately after the samples were taken out of a dry box, and the duration of each experiment was kept unchanged. During the experiments, the airflow was adjusted by an inverter speed control unit, and the air velocity was measured by an anemometer (Model 9565, TSI, USA). The height of the velocity measurement point from the holder surface was 75 mm. It was ensured that the airflow entering the working section (cross-

sectional area: 304 mm × 304 mm) was steady in both magnitude and direction. The flexible substrate with deposited particles was placed in the working section. One end of the flexible substrate was affixed to the holder (Figure 1b). The free end which was naturally drooping due to its own weight in the absence of airflow, was then lifted by the airflow and gradually straightened at air velocities below the critical air velocity, and finally began fluttering above the critical air velocity. The effective test area of the fluttering substrate sized 80 mm × 30 mm contained four marked positions (P1, P2, P3, P4) set at 20 mm, 40 mm, 60 mm, and 80 mm from the fixed end respectively (Figure 1c). A high-speed camera (VEO-L, Phantom, USA) was used to capture the substrate fluttering behavior by tracking the marked positions (Figure 1b). It was installed beside the wind tunnel to capture the sideview of the fluttering substrate. The movements of the four marked positions on the fluttering substrate were recorded by the high-speed camera at 5000 frames per second (5000 fps) for subsequent motion analysis. The footage was processed to determine the frequency, displacement, and acceleration of the fluttering substrate. The fluttering frequency was defined as the number of fluttering cycles within one second. The displacements of the marked positions were expressed as $x(t)$ and $y(t)$. The fluttering acceleration components a_x (x-direction) and a_y (y-direction) were then calculated. The fluttering acceleration was the modulus calculated from both components. The maximum acceleration during experiments was selected as the fluttering acceleration in this paper.

Figure 1

The particles were randomly deposited by gravity in a monolayer at the four positions on the top surface of the flexible substrate in preparation for the particle resuspension experiments (Figure 1c). To avoid biasing the resuspension results by the non-fluttering substrate and undesired particles that could be easily removed, the particle-laden substrate was placed in the wind tunnel for 3 minutes with an airflow below the critical velocity before the experiments. During the experiments, the number of particles remaining on the substrate at each air velocity (after a duration of 3 minutes including a transient period of about 5 seconds for the air velocity to reach the target velocity from 0 m/s) was observed with a microscope (Ni-E, Nikon, Japan) to assess particle resuspension. Figure 2 shows some microscope photos in the fluttering substrate case used to determine the remaining fraction, which was defined as the ratio of the number of remaining particles at air velocity U to that at U = 0 m/s. The remaining fraction dropped to 0 at U = 8 m/s, indicating that all particles were resuspended (Figure 2). In order to reduce the uncertainty, the number of particles deposited in the observation zone at each position was more than 100 and in the same

order of magnitude for the four diameters. Each test was triplicated under the same experimental conditions. The above-mentioned particle deposition and observation procedures were consistent in all resuspension experiments in the present work, including fixed substrate experiments, centrifugal experiments, and vibration experiments.

Figure 2

In the fixed substrate case, the same flexible substrate was wholly adhered to a flat surface so it would not flutter under the same experimental conditions. Unlike its fluttering counterpart, the influence of different positions on particle resuspension was minimized as the fixed substrate was stationary. Theoretical analysis of the mean values of forces/moments and repeated experimental results also show that the particle resuspension hardly occurred in the fixed substrate case under our experimental conditions (Figure S1). Therefore, in this case, the position effects were negligible and the moderate results at midpoint (P2) of the effective test area were selected as a representative to contrast the particle resuspension between fixed and fluttering substrates.

3. Results and discussion

3.1 Flow-induced flutter of flexible substrate

The flow-induced flutter of the flexible substrate is discussed in this section. The substrate began to flutter at air velocity U = 3 m/s which is the critical air velocity in the present work. Figure 3 shows a series of photos at different instants of the fluttering substrate to demonstrate the process of flutter at the critical air velocity. The four marked positions and the fixed end (position 0) are displayed, which clearly reflects the overall motion of the substrate. It can also be observed that the free end of the fluttering substrate underwent some rapid positional changes that completed a cycle within 50 ms. Figure 4 presents the stacked images of traces within one second of the fluttering substrate to visualize the differences in motion between the positions at different air velocities. It is evident that the fluttering amplitude increased from P1 to P4 at all air velocities (Figure 4). Another finding was that the increasing air velocity led to more sudden deviations from the periodic flutter. Movements of P3 and P4 were most affected by the air velocity, while P1 and P2 moved more periodically.

Figure 3

Figure 4

The fluttering frequency of the substrate is plotted as a function of the air velocity in Figure 5a. Within the range of air velocity selected in this study, it was found that there existed a linear relationship between the fluttering frequency f and the air velocity U, which is consistent with the findings of Olsen et al. [34] and Xu et al. [35]. Figure 5b shows the fluttering acceleration a_F at different positions and air velocities U. At lower air velocities of 3 m/s and 4 m/s, the acceleration at each marked position remained nearly constant with the increasing air velocity. The acceleration at P4 started to rise sharply at U = 5 m/s, reaching a maximum of almost 70000 m/s^2 at U = 8 m/s. As shown in Figure 4, the motion trace of P4 became chaotic at U = 5 m/s and thereafter became more disordered at faster air velocities, resulting in a higher acceleration. Furthermore, the traces at P3 and P4 overlapped at air velocities larger than U = 6 m/s and were more disordered than those at P1 and P2 at higher air velocities, signifying a surge in their accelerations (Figure 5b). Moreover, at U = 3 and 4 m/s, the accelerations at P1 and P3 were higher than those at P2 and P4, respectively, but as the flutter became vigorous at U = 7 and 8 m/s, the acceleration showed a noticeable increasing trend from P1 to P4. Over the air velocity range of 3 ~ 8 m/s, the acceleration at P4 changed the most, followed by P3 and P2, while the acceleration at P1 hardly changed.

Figure 5

3.2 Particle resuspension

Experimental results of particle resuspension from the fluttering substrate and the fixed substrate are compared in this section. The mean results of the triplicate tests of the remaining fraction for particles with the four diameters are plotted in Figure 6 with error bars representing standard deviation. There was almost no particle resuspension in the fixed substrate case with a remaining fraction of 1 ~ 0.9786, while the local remaining fraction could be reduced from 1 to 0 in the fluttering substrate case. These results indicate that the flow-induced flutter could significantly enhance particle resuspension compared with the fixed substrate case, but the enhancement tended to 0 with the decreasing particle diameter. For the fluttering substrate case, particle diameter, position, and air velocity were found to be important factors influencing the particle resuspension. First, larger particles were resuspended more, and the smallest 6-μm particles were the most difficult to be resuspended. This finding was consistent with the generalization of Hinds [36]. Secondly, there was a trend of incremental particle resuspension from P1 to P4, which matched well with the trend of increasing fluttering amplitude mentioned in Section 3.1. P4 always had the most significant particle

resuspension, followed by P3. The larger air velocity led to more particle resuspension in most cases, but the relationship was not linear.

Figure 6

The threshold velocity, defined as the air velocity at which the remaining fraction equaled 0.5, was employed to evaluate the effects of the studied parameters. The results for those cases where the remaining fraction could reach 0.5 under our experimental conditions imply that the flutter of the substrate could greatly reduce the threshold velocity compared with the fixed substrate, and the threshold velocity decreased from P1 to P4 and with increasing particle diameter.

3.3 Forces acting on a particle

In this section, the forces acting on a particle on the substrate under the influence of airflow (Figure 7), are analyzed, including adhesive force F_A between the particle and the substrate, drag force F_{D0}, lift force F_{L0} in the fixed substrate case, and force caused by the fluttering acceleration F_F generated only in the fluttering substrate case. The gravitational force *mg* acting on the micron-sized particle used in our cases was several orders of magnitude smaller than the adhesive force F_A. It is thus neglected here.

Figure 7

3.3.1 Adhesive force

The adhesive force F_A can be directly measured by the centrifugal method as identified in previous work by our group [37, 38]. This method approximates the mean value of adhesive force as the centrifugal force required to remove 50% of particles with the same diameter. However, the limited speed of the centrifuge (Z207A, Hermle, Germany) employed in the present work was insufficient to complete the measurement for all particle sizes. Therefore, only the adhesive forces for the particles with diameters of 39 μm and 51 μm were directly measured in this study. Corn [39] experimentally found that the adhesive force between particles and surfaces at a given relative humidity was directly proportional to the particle diameter. Hinds [36] also generalized a proportional relationship between the adhesive force and the particle diameter. Thus, the adhesive forces for other particle sizes were predicted based on a linear fitted equation as follows:

$$F_A = 0.02237 d_P \ (6\ \mu m \le d_P \le 51\ \mu m) \quad (1)$$

where F_A is the adhesive force between particles and the substrate for the present work, and d_P is the particle diameter. The results of the centrifuge experiment together with the linear regression are plotted in Figure 8. The experimental results are in good agreement with the regression. It should be noted that the measured

adhesive force in this work was the overall force including the effects of relative humidity, capillary force, surface roughness and other possible effects [40-42].

Figure 8

3.3.2 Drag and lift forces in the fixed substrate case

Determining the aerodynamic forces (drag force and lift force) acting on a particle in the fluttering substrate case, like in this experiment, is outside the capacity. Therefore, the aerodynamic forces (F_{D0} and F_{L0}) in the fixed substrate case were analyzed to help provide the basis for the analysis of the fluttering substrate case. Since the Reynolds number was significantly less than 5×10^5, the drag force F_{D0} and lift force F_{L0} could be determined by a simple shear-flow model. The drag force F_{D0} is estimated according to the following equation [43]:

$$F_{D0} = 3\pi\mu u_P d_P f_W \tag{2}$$

where μ is the dynamic viscosity of air at 26.8 ℃, u_P is the air velocity at the level of the particle center, and f_W = 1.7009 is the factor accounting for the wall effect. The velocity u_P can be found by the velocity profile [44]:

$$\frac{u_P}{U} = \frac{3}{2}\frac{r_P}{\delta} - \frac{1}{2}\left(\frac{r_P}{\delta}\right)^3 \tag{3}$$

$$\delta = 5.0\frac{x}{\sqrt{Re_x}} = 5.0\frac{x}{\sqrt{\frac{Ux}{\nu}}} \tag{4}$$

where r_P is the particle radius, δ is the boundary layer thickness, Re_x is the Reynolds number, x = 0.06 m (including the P2 distance from the fixed end and the length of the fixed end as shown in Figure 1c, so x = 0.04 + 0.02 = 0.06 m), and ν is the kinematic viscosity of air at 26.8 ℃. The lift force F_{L0} is calculated as [45]:

$$F_{L0} = 9.22(\dot{\gamma}\mu r_P^2)\left(\frac{\dot{\gamma} r_P^2}{\nu}\right) \tag{5}$$

where $\dot{\gamma}$ is the shear rate.

3.3.3 Force caused by the fluttering acceleration

The acceleration of the fluttering substrate can generate a force acting on the particles, as demonstrated by the red arrow in Figure 7. Since the maximum acceleration was measured to be three orders

of magnitude larger than gravitational acceleration, it could be very important to particle resuspension. The associated force F_F can be calculated by a simple expression:

$$F_F = ma_F \tag{6}$$

where m is the mass of a particle and a_F is the fluttering acceleration. Based on the calculated results in *Section 3.3.2* and *3.3.3*, it was found that the force F_F was much larger than the drag force F_{D0} and the lift force F_{L0} by at least an order of magnitude under the same conditions. As such, it would be one of the main causes for enhancing the particle resuspension when the substrate was switched from fixed to fluttering.

3.3.4 Comparison between the acceleration-induced force and adhesive force

Figure 9 demonstrates a direct comparison between the force F_F and the adhesive force F_A. The force F_F was larger than the adhesive force F_A only for the 31-μm particles at P4 and the 51-μm particles at P3 and P4. However, it was observed that the particles had been significantly resuspended even though the force F_F was less than the adhesive force F_A (circled in Figure 9). Recalling the findings in Sections 3.1 and 3.2, unlike the fluttering acceleration, the particle resuspension generally increased from P1 to P4. It was thus inferred that the particle resuspension was not positively correlated with the force F_F. To sum up, these findings suggested that the force F_F was an important factor contributing to the particle resuspension in the fluttering substrate case, but certainly not the only one.

Figure 9

3.4 Force and moment analysis of particle resuspension from the fluttering substrate

Particle resuspension can be demonstrated as a competition between removal and adhesive forces/moments acting on the particle due to the negligible gravitational force (Figure 7). The mechanisms initiating particle resuspension are explored in this section by the static force and moment balance analysis. There are three possible modes of particle incipient motion in the fixed substrate case: lift-off, sliding, and rolling. The aerodynamic forces (F_{D0} and F_{L0}) of the fixed substrate case were tentatively applied to the fluttering substrate case. The corresponding formulas of force/moment analysis including the force F_F for three modes are respectively (as follows):

$$F_{L0} + F_F > F_A \tag{7}$$

$$F_{D0} > \mu_S(F_A - F_{L0} - F_F) \tag{8}$$

$$1.4r_P F_{D0} + aF_{L0} + aF_F > aF_A \tag{9}$$

where μ_S is the static friction coefficient, 1.4 is the factor accounting for the presence of the substrate [1], a is the contact radius that can be evaluated by the JKR model [20, 23, 46] describing the contact of elastic solids:

$$a = \left(\frac{6\pi W_A r_P^2}{K}\right)^{\frac{1}{3}} = \left(\frac{12\pi\sqrt{\gamma_1\gamma_2}r_P^2}{K}\right)^{\frac{1}{3}} \tag{10}$$

where W_A is the work of adhesion that can be converted into the form of the surface energy [17, 47], γ_i is the surface energy (i = 1 is for particle and i = 2 is for substrate), and K is the composite Young's modulus defined as:

$$K = \frac{4}{3}\left[\frac{(1-\nu_1^2)}{E_1} + \frac{(1-\nu_2^2)}{E_2}\right]^{-1} \tag{11}$$

where E_i is the Young's modulus and ν_i is the Poisson's ratio. In this study, γ_1 = 0.042 J/m^2, γ_2 = 0.030 J/m^2, E_1 = 3.2 × 10^9 N/m^2, E_2 = 1.5 × 10^9 N/m^2, ν_1 = 0.35, and ν_2 = 0.43. It is noted that Eq. (7) ~ (9) are for the fixed substrate case when the force F_F is equal to 0. Eq. (9) is a moment comparison where the terms on the left-hand side are the aerodynamic moment in the fixed substrate case denoted by $M(F_0)$, i.e., $1.4r_PF_{D0}$ + aF_{L0}, and the moment of the force F_F denoted by $M(F_F)$, and the term on the right-hand side is the adhesive moment denoted by $M(F_A)$. Eq. (8) and Eq. (9) actually have a similar form. When Eq. (8) is equivalent to Eq. (9), μ_S is equal to $a/1.4r_P$. In this study, $a/1.4r_P$ was less than 0.03. Theoretically, the sliding mode is less important than the rolling mode in the present work. It was also confirmed by the previous experimental investigation that rolling was the primary mode [6]. However, as shown in Figure 7, the force F_F might contribute a lot to the lift-off mode, which cannot be ignored here. Thus, only the lift-off mode (force analysis) and the rolling mode (moment analysis) are reported in this section. The forces/moments acting on the particles, which were transformed from the experimental data by Eq. (7) or Eq. (9), are displayed with their corresponding remaining fraction results in Figure 10 and 11.

3.4.1 Lift-off mode

Figure 10 presents the force analysis for the lift-off mode in the fluttering substrate case. The two dashed lines form a dashed box with the x- and y-axis. Within the dashed box, the adhesive force F_A is not overcome but the remaining fraction drops below 0.5. As depicted in Figure 10, most plots below the remaining fraction of 0.5 were within the dashed box, except for very few plots with the remaining fraction

of almost 0 when the adhesive force was overcome. It indicates that the $F_F + F_{L0}$ failed to explain the particle resuspension in the fluttering substrate case by the force analysis for the lift-off mode.

Figure 10

3.4.2 Rolling mode

Figure 11 demonstrates the moment analysis for the rolling mode in the fluttering substrate case with dashed boxes equivalent to those for the force analysis. Similar conclusions can be drawn from Figure 11. The combination of the force F_F and the aerodynamic forces (F_{D0} and F_{L0}) in the fixed substrate case failed to explain the actual situation of particle resuspension, both in the lift-off mode and rolling mode, in the fluttering substrate case. Therefore, compared with the fixed substrate case, the aerodynamic forces/moments acting on the particles must be enhanced in the fluttering substrate case, which was speculated to be another necessary factor enhancing the particle resuspension. This aerodynamic force/moment enhancement could be attributed to the coupling of the flow-induced flutter of the substrate and its resulting turbulent flow. Furthermore, as estimated from Figure 10 and Figure 11, the aerodynamic force/moment enhancement would be comparable to or even greater than its force F_F/moment $M(F_F)$ counterpart in the fluttering substrate case. It is noted that the enhancement could be calculated from Eq. (7) and (9).

Figure 11

3.4.3 Additional supporting evidence

Since the fluttering substrate case involves the coupled effects of airflow and substrate vibration, it is necessary to quantify the two separately through additional parametric tests to verify our calculations. One is the fixed substrate case mentioned above, and the other is a vertical vibration experiment without the air motion under the same experimental conditions. It is noted that the substrate cannot flutter in the vibration experiment. Details are presented in Supplementary Material.

The force/moment analysis for the lift-off mode/rolling mode in the fixed substrate case is shown in Figure S1. These results indicate that it was almost impossible for lift-off mode to occur in this case because the lift force F_{L0} was several orders of magnitude smaller than the threshold (Figure S1a). Insufficient moments (Figure S1b) also agreed with the experimental results of particle resuspension, but the gap from the threshold was much smaller than that in the lift mode. It in turn implies that the rolling mode was the more likely mechanism to trigger the particle resuspension in this case.

The setup of the vibration experiment is schematically shown in Figure S2. The results are compared with those of the fluttering experiment (U = 3 m/s, P4) in Figure S3. Except for the 6μm- and 13μm-particles that failed to be resuspended in both experiments, the reductions in remaining fraction of other particles in the fluttering case were more than double those in the vibration case, even though the acceleration a_V measured in the latter was higher than the acceleration a_F in the former. These results support our conclusions presented in *Section 3.3.3* and *Section 3.4.2*.

3.5 Implications and limitations

The results of this work can have practical implications in several fields. In the industrial field, fluttering dynamics is expected to inform applications that require particle resuspension, e.g., aerosolization of powders, drug delivery, spray systems and surface contaminant cleaning, due to its strong resuspension capacity. The findings of this paper on wind speed, particle size and position also benefit the optimization of related products. In the environmental field, our experimental results indicate that substrate flutter can cause significant particle resuspension in low-air-velocity scenarios, which may easily lead to air pollution. Besides, liquid aerosol resuspension from the fluttering substrates warrants further investigation. Although liquid aerosols are more difficult to be resuspended than solid particles [37], it can be speculated from this paper that the substrate flutter may achieve appreciable liquid aerosol resuspension. Its in-depth understanding may help reduce the transmission of pathogens via respiratory droplets.

Some limitations exist in the present work. Different substrates with different materials and sizes have different critical air velocities for fluttering. Furthermore, in real-life scenarios, the flutter phenomenon is complex, subject to factors such as different shapes of substrates and fluctuating airflow [48-50]. This work only chose one substrate material and simplified conditions to study the effects of flutter on particle resuspension and the underlying mechanisms. The results provide useful information but cannot be directly applied to industrial products or environmental scenarios. The aerodynamic force/moment enhancement calculated in the present work was speculated to be caused by the coupling of the flow-induced flutter of the substrate and its resulting turbulent flow; further investigation of the airflow dynamics surrounding the fluttering substrate and the stochastic nature of the resuspension problem [12, 18, 51] is required for a more thorough understanding of flutter-induced particle resuspension enhancement.

4. Conclusions

This paper presented an experimental study on the resuspension of polystyrene (PS) spherical particles from a flow-induced fluttering flexible oriented polypropylene (OPP) substrate at air velocities of 0 ~ 8 m/s with a comparative fixed substrate experiment under the same conditions. The fluttering motion of the substrate was quantified by a high-speed camera, and the particle resuspension was assessed by a microscope. There was almost no particle resuspension in the fixed substrate case with a remaining fraction of 1 ~ 0.9786, while the local remaining fraction could be reduced from 1 to 0 in the fluttering substrate case, showing a remarkable particle resuspension enhancement and a great reduction in the threshold velocity, which were dependent on the particle diameter and position. For a single particle in the fluttering substrate case, the force caused by the fluttering acceleration of the substrate, which exceeded its gravity by several orders of magnitude, was identified as an important factor enhancing the particle resuspension. Another necessary factor was the significant flutter-induced aerodynamic force/moment enhancement acting on the particle, illustrated by the static force and moment balance analysis.

Supplementary material

Figures S1, S2 and S3.

Nomenclature

a	Contact radius [m]
a_F	Fluttering acceleration (maximum) of the substrate [m/s^2]
a_V	Vibration acceleration of the substrate [m/s^2]
a_x	Acceleration component along the x-axis [m/s^2]
a_y	Acceleration component along the y-axis [m/s^2]
d_P	Particle diameter [m]
E_1	Young's modulus of the particle [N/m^2]
E_2	Young's modulus of the substrate [N/m^2]
f	Fluttering frequency [Hz]
f_W	Factor accounting for the wall effect
F_A	Adhesive force [N]

F_{D0}	Drag force in the fixed substrate case [N]
F_F	Force caused by the fluttering acceleration of the substrate [N]
F_{L0}	Lift force in the fixed substrate case [N]
g	Gravitational acceleration [m/s^2]
K	Composite Young's modulus [N/m^2]
m	Mass [kg]
$M(F_A)$	Moment of the adhesive force [N·m]
$M(F_0)$	Moment of the drag and lift forces in the fixed substrate case [N·m]
O	Rolling point
R^2	Coefficient of determination
Re_x	Reynolds number
r_P	Particle radius [m]
t	Time [s]
U	Air velocity [m/s]
u_P	Air velocity at the level of the particle center [m/s]
W_A	Work of adhesion [J/m^2]
x	Cartesian coordinate [m]
y	Cartesian coordinate [m]
γ_1	Surface energy of the particle [J/m^2]
γ_2	Surface energy of the substrate [J/m^2]
$\dot{\gamma}$	Shear rate [s^{-1}]
μ	Dynamic viscosity of air [N·s/m^2]
μ_S	Static friction coefficient
ν	Kinematic viscosity [m^2/s]
ν_1	Poisson's ratio of the particle
ν_2	Poisson's ratio of the substrate
δ	Boundary layer thickness [m]

Declaration of competing interest

The authors declare that they have no known competing financial interests or personal relationships that could have appeared to influence the work reported in this paper.

Funding

This work was supported by the General Research Fund (GRF) (project no. 17203220) and the Collaborative Research Fund (CRF) (project no. C1105-20G) granted by the Research Grants Council of the Hong Kong Special Administrative Region, China.

ORCID

Jie Feng, https://orcid.org/0000-0001-7918-4612.

Cunteng Wang, https://orcid.org/0000-0002-3014-8407.

Yi Zhang, https://orcid.org/0000-0003-3630-2759.

Ka Chung Chan, https://orcid.org/0000-0003-1944-1175.

Chun Ho Liu, https://orcid.org/0000-0002-4609-524X.

Christopher Y.H. Chao, https://orcid.org/0000-0002-2974-0403.

Sau Chung Fu, https://orcid.org/0000-0003-2861-7582.

References

[1] Henry C., & Minier J.P. Progress in particle resuspension from rough surfaces by turbulent flows. Progress in Energy and Combustion Science. 2014. 45:1-53. https://doi.org/10.1016/j.pecs.2014.06.001.

[2] Choi H.S., & Hwang J. Reduction of submicron-sized aerosols emission in electrostatic precipitation by electrical attraction with micron-sized aerosols. Powder Technology. 2021. 377:882-9. https://doi.org/10.1016/j.powtec.2020.09.031.

[3] Troiano M., Salatino P., Solimene R., & Montagnaro F. Wall effects in entrained particle-laden flows: The role of particle stickiness on solid segregation and build-up of wall deposits. Powder Technology. 2014. 266:282-91. https://doi.org/10.1016/j.powtec.2014.06.039.

[4] Chiou S.F., & Tsai C.J. Measurement of emission factor of road dust in a wind tunnel. Powder Technology. 2001. 118(1-2):10-5. https://doi.org/10.1016/s0032-5910(01)00289-3.

[5] Wu Y.L., Davidson C.I., & Russell A.G. Controlled wind-tunnel experiments for particle bounceoff and resuspension. Aerosol Science and Technology. 1992. 17(4):245-62. https://doi.org/10.1080/02786829208959574.

[6] Ibrahim A.H., Dunn P.F., & Brach R.M. Microparticle detachment from surfaces exposed to turbulent air flow: Controlled experiments and modeling. Journal of Aerosol Science. 2003. 34(6):765-82. https://doi.org/10.1016/s0021-8502(03)00031-4.

[7] Jiang Y.B., Matsusaka S., Masuda H., & Qian Y. Characterizing the effect of substrate surface roughness on particle-wall interaction with the airflow method. Powder Technology. 2008. 186(3):199-205. https://doi.org/10.1016/j.powtec.2007.11.041.

[8] Barth T., Preuß J., Müller G., & Hampel U. Single particle resuspension experiments in turbulent channel flows. Journal of Aerosol Science. 2014. 71:40-51. https://doi.org/10.1016/j.jaerosci.2014.01.006.

[9] Kim Y., Wellum G., Mello K., Strawhecker K.E., Thoms R., Giaya A., & Wyslouzil B.E. Effects of relative humidity and particle and surface properties on particle resuspension rates. Aerosol Science and Technology. 2016. 50(4):339-52. https://doi.org/10.1080/02786826.2016.1152350.

[10] Rondeau A., Peillon S., Vidales A.M., Benito J., Unac R., Sabroux J.C., & Gensdarmes F. Evidence of inter-particles collision effect in airflow resuspension of poly-dispersed non-spherical tungsten particles in monolayer deposits. Journal of Aerosol Science. 2021. 154:16. https://doi.org/10.1016/j.jaerosci.2020.105735.

[11] Ziskind G., Fichman M., & Gutfinger C. Adhesion moment model for estimating particle detachment from a surface. Journal of Aerosol Science. 1997. 28(4):623-34. https://doi.org/10.1016/s0021-8502(96)00460-0.

[12] Reeks M.W., & Hall D. Kinetic models for particle resuspension in turbulent flows: Theory and measurement. Journal of Aerosol Science. 2001. 32(1):1-31. https://doi.org/10.1016/s0021-8502(00)00063-x.

[13] Tran-Cong S., Gay M., & Michaelides E.E. Drag coefficients of irregularly shaped particles. Powder Technology. 2004. 139(1):21-32. https://doi.org/10.1016/j.powtec.2003.10.002.

[14] Fillingham P., Vaddi R.S., Bruning A., Israel G., & Novosselov I.V. Drag, lift, and torque on a prolate spheroid resting on a smooth surface in a linear shear flow. Powder Technology. 2021. 377:958-65. https://doi.org/10.1016/j.powtec.2020.09.042.

[15] Guingo M., & Minier J.P. A new model for the simulation of particle resuspension by turbulent flows based on a stochastic description of wall roughness and adhesion forces. Journal of Aerosol Science. 2008. 39(11):957-73. https://doi.org/10.1016/j.jaerosci.2008.06.007.

[16] Goldasteh I., Ahmadi G., & Ferro A.R. Monte carlo simulation of micron size spherical particle removal and resuspension from substrate under fluid flows. Journal of Aerosol Science. 2013. 66:62-71. https://doi.org/10.1016/j.jaerosci.2013.07.012.

[17] You S.M., & Wan M.P. A new turbulent-burst-based model for particle resuspension from rough surfaces in turbulent flow. Aerosol Science and Technology. 2014. 48(10):1031-42. https://doi.org/10.1080/02786826.2014.955908.

[18] Olivares M.C.V., Benito J.G., Unac R.O., & Vidales A.M. Kinetic monte carlo method applied to micrometric particle detachment mechanisms by aerodynamic forces. Journal of Physics-Condensed Matter. 2022. 34(7):17. https://doi.org/10.1088/1361-648X/ac3690.

[19] Nasr B., Ahmadi G., Ferro A.R., & Dhaniyala S. A model for particle removal from surfaces with large-scale roughness in turbulent flows. Aerosol Science and Technology. 2020. 54(3):291-303. https://doi.org/10.1080/02786826.2019.1692126.

[20] Ziskind G., Fichman M., & Gutfinger C. Particle behavior on surfaces subjected to external excitations. Journal of Aerosol Science. 2000. 31(6):703-19. https://doi.org/10.1016/s0021-8502(99)00554-6.

[21] Hein K., Hucke T., Stintz M., & Ripperger S. Analysis of adhesion forces between particles and wall based on the vibration method. Particle & Particle Systems Characterization. 2002. 19(4):269-76. https://doi.org/10.1002/1521-4117(200208)19:4<269::Aid-ppsc269>3.0.Co;2-t.

[22] Hubbard J.A., Brockmann J.E., Rivera D., & Moore D.G. Experimental study of impulse resuspension with laser doppler vibrometry. Aerosol Science and Technology. 2012. 46(12):1303-12. https://doi.org/10.1080/02786826.2012.708464.

[23] Chatoutsidou S.E., & Lazaridis M. Resuspension of spherical particles due to surface vibration. Particuology. 2021. 54:126-35. https://doi.org/10.1016/j.partic.2020.08.003.

[24] Wang J.H., Niu L.M., Zhang T.F., & Wang S.G. Detachment of adhered particles from a cloth surface subjected to a rod strike. Aerosol Science and Technology. 2019. 53(4):435-48. https://doi.org/10.1080/02786826.2019.1569199.

[25] Argentina M., & Mahadevan L. Fluid-flow-induced flutter of a flag. Proceedings of the National Academy of Sciences of the United States of America. 2005. 102(6):1829-34. https://doi.org/10.1073/pnas.0408383102.

[26] Virot E., Amandolese X., & Hemon P. Fluttering flags: An experimental study of fluid forces. Journal of Fluids and Structures. 2013. 43:385-401. https://doi.org/10.1016/j.jfluidstructs.2013.09.012.

[27] Zhang Y., Fu S.C., Chan K.C., Shin D.M., & Chao C.Y.H. Boosting power output of flutter-driven triboelectric nanogenerator by flexible flagpole. Nano Energy. 2021. 88:12. https://doi.org/10.1016/j.nanoen.2021.106284.

[28] Zhong X.L., Fu S.C., Chan K.C., Yang G., Qiu H.H., & Chao C.Y.H. Experimental study on the thermal-hydraulic performance of a fluttering split flag in a channel flow. International Journal of Heat and Mass Transfer. 2022. 182:10. https://doi.org/10.1016/j.ijheatmasstransfer.2021.121945.

[29] Giess P., Goddard A.J.H., & Shaw G. Factors affecting particle resuspension from grass swards. Journal of Aerosol Science. 1997. 28(7):1331-49. https://doi.org/10.1016/s0021-8502(97)00021-9.

[30] Petroff A., Zhang L.M., Pryor S.C., & Belot Y. An extended dry deposition model for aerosols onto broadleaf canopies. Journal of Aerosol Science. 2009. 40(3):218-40. https://doi.org/10.1016/j.jaerosci.2008.11.006.

[31] Zhang X.Y., Lyu J.Y., Han Y.J., Sun N.X., Sun W., Li J.M., Liu C.J., & Yin S. Effects of the leaf functional traits of coniferous and broadleaved trees in subtropical monsoon regions on pm2.5 dry deposition velocities. Environmental Pollution. 2020. 265:10. https://doi.org/10.1016/j.envpol.2020.114845.

[32] Selvam P., McNair D., Truman R., & Smyth H.D.C. A novel dry powder inhaler: Effect of device design on dispersion performance. International Journal of Pharmaceutics. 2010. 401(1-2):1-6. https://doi.org/10.1016/j.ijpharm.2010.07.056.

[33] Selvam P., Marek S., Truman C.R., McNair D., & Smyth H.D.C. Micronized drug adhesion and detachment from surfaces: Effect of loading conditions. Aerosol Science and Technology. 2011. 45(1):81-7. https://doi.org/10.1080/02786826.2010.522628.

[34] Olsen M., Zhang R.Y., Ortegren J., Andersson H., Yang Y., & Olin H. Frequency and voltage response of a wind-driven fluttering triboelectric nanogenerator. Scientific Reports. 2019. 9:6. https://doi.org/10.1038/s41598-019-42128-7.

[35] Xu M.Y., Wang Y.C., Zhang S.L., Ding W.B., Cheng J., He X., Zhang P., Wang Z.J., Pan X.X., & Wang Z.L. An aeroelastic flutter based triboelectric nanogenerator as a self-powered active wind speed sensor in harsh environment. Extreme Mechanics Letters. 2017. 15:122-9. https://doi.org/10.1016/j.eml.2017.07.005.

[36] Hinds W.C. Aerosol technology: Properties, behavior, and measurement of airborne particles. 2nd ed: Wiley. 1999.

[37] Leung W.T., Fu S.C., Sze To G.N., & Chao C.Y.H. Comparison of the resuspension behavior between liquid and solid aerosols. Aerosol Science and Technology. 2013. 47(11):1239-47. https://doi.org/10.1080/02786826.2013.831973.

[38] Leung W.T., Fu S.C., & Chao C.Y.H. Detachment of droplets by air jet impingement. Aerosol Science and Technology. 2017. 51(4):467-76. https://doi.org/10.1080/02786826.2016.1265911.

[39] Corn M. The adhesion of solid particles to solid surfaces ii. Journal of the Air Pollution Control Association. 1961. 11(12):566-84. https://doi.org/10.1080/00022470.1961.10468039.

[40] Ibrahim A.H., Dunn P.F., & Brach R.M. Microparticle detachment from surfaces exposed to turbulent air flow: Effects of flow and particle deposition characteristics. Journal of Aerosol Science. 2004. 35(7):805-21. https://doi.org/10.1016/j.jaerosci.2004.01.002.

[41] Rabinovich E., & Kalman H. Incipient motion of individual particles in horizontal particle-fluid systems: A. Experimental analysis. Powder Technology. 2009. 192(3):318-25. https://doi.org/10.1016/j.powtec.2009.01.013.

[42] Peillon S., Autricque A., Redolfi M., Stancu C., Gensdarmes F., Grisolia C., & Pluchery O. Adhesion of tungsten particles on rough tungsten surfaces using atomic force microscopy. Journal of Aerosol Science. 2019. 137:12. https://doi.org/10.1016/j.jaerosci.2019.105431.

[43] O'Neill M.E. A sphere in contact with a plane wall in a slow linear shear flow. Chemical Engineering Science. 1968. 23(11):1293-8. https://doi.org/10.1016/0009-2509(68)89039-6.

[44] Holman J.P. Heat transfer. 8th ed: Mcgraw-Hill College. 1997.

[45] Leighton D., & Acrivos A. The lift on a small sphere touching a plane in the presence of a simple shear flow. Journal of Applied Mathematics and Physics (ZAMP). 1985. 36:174-8. https://doi.org/10.1007/BF00949042.

[46] Johnson K.L., Kendall K., & Roberts A.D. Surface energy and the contact of elastic solids. Proceedings of the Royal Society of London, Series A. 1971. 324(1558):301-13. https://doi.org/10.1098/rspa.1971.0141.

[47] Israelachvili J.N. Intermolecular and surface forces. 3rd ed: Academic Press. 2011.

[48] Ibrahim A.H., & Dunn R.F. Effects of temporal flow acceleration on the detachment of microparticles from surfaces. Journal of Aerosol Science. 2006. 37(10):1258-66. https://doi.org/10.1016/j.jaerosci.2006.01.007.

[49] Benito J.G., Unac R.O., Vidales A.M., & Ippolito I. Kinetic programmed resuspension - kpr technique. Journal of Aerosol Science. 2018. 122:21-31. https://doi.org/10.1016/j.jaerosci.2018.05.006.

[50] Theron F., Debba D., & Le Coq L. Influence of the transient airflow pattern on the temporal evolution of microparticle resuspension: Application to ventilated duct during fan acceleration. Aerosol Science and Technology. 2022. 56(11):1033-46. https://doi.org/10.1080/02786826.2022.2120793.

[51] Wen H.Y., & Kasper G. On the kinetics of particle reentrainment from surfaces. Journal of Aerosol Science. 1989. 20(4):483-98. https://doi.org/10.1016/0021-8502(89)90082-7.

Table

Particle resuspension from a flow-induced fluttering flexible substrate

Jie Feng [a], Cunteng Wang [a], Yi Zhang [a], Ka Chung Chan [a], Chun Ho Liu [a], Christopher Y.H. Chao [b, c], Sau Chung Fu [b, *]

[a] Department of Mechanical Engineering, The University of Hong Kong, Hong Kong, China

[b] Department of Building Environment and Energy Engineering, The Hong Kong Polytechnic University, Hong Kong, China

[c] Department of Mechanical Engineering, The Hong Kong Polytechnic University, Hong Kong, China

[*] Corresponding author. E-mail address: schung.fu@polyu.edu.hk (S.C. Fu).

Table 1. Material properties of particle and substrate

Material properties	Particle	Substrate
Surface energy [J/m^2]	0.042	0.030
Young's modulus [N/m^2]	3.2×10^9	1.5×10^9
Poisson's ratio	0.35	0.43

Figures

Particle resuspension from a flow-induced fluttering flexible substrate

Jie Feng [a], Cunteng Wang [a], Yi Zhang [a], Ka Chung Chan [a], Chun Ho Liu [a], Christopher Y.H. Chao [b, c], Sau Chung Fu [b, *]

[a] Department of Mechanical Engineering, The University of Hong Kong, Hong Kong, China

[b] Department of Building Environment and Energy Engineering, The Hong Kong Polytechnic University, Hong Kong, China

[c] Department of Mechanical Engineering, The Hong Kong Polytechnic University, Hong Kong, China

[*] Corresponding author. E-mail address: schung.fu@polyu.edu.hk (S.C. Fu).

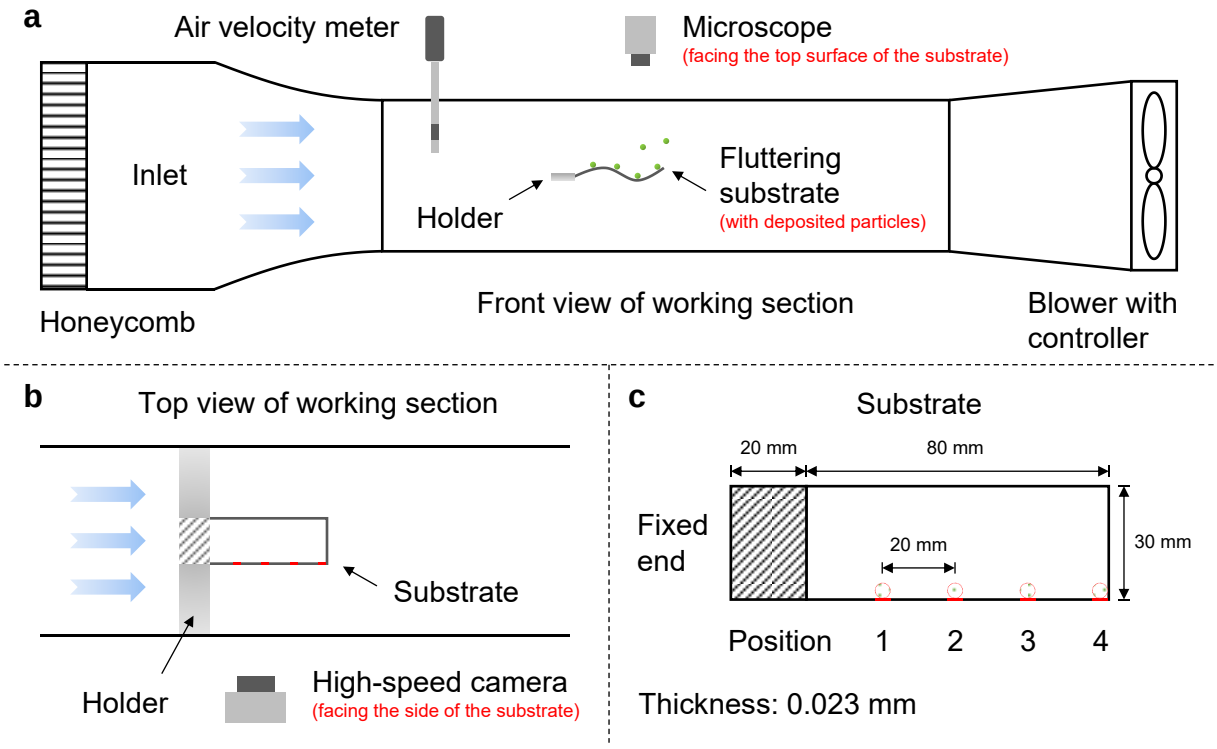

Figure 1. Schematic diagram of the experimental setup. **a,** The wind tunnel for particle resuspension experiments (the particles drawn here are exaggerated for illustration only). **b,** Top view of the working section of wind tunnel. **c,** The substrate and four marked positions (P1, P2, P3, P4). The four marks on the side were used for high-speed camera tracking and the particles were deposited within the corresponding red dotted circles on the top surface for observation. The observation zones were ensured to be consistent for each experiment.

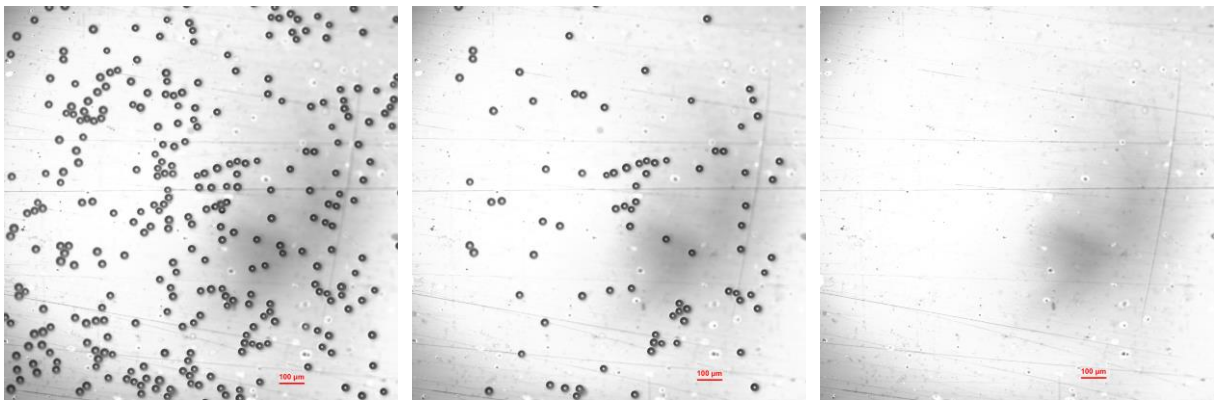

Figure 2. Microscope photos of particles with a diameter of 31 μm at P4 at different air velocities *U* after 3 minutes of exposure to airflow.

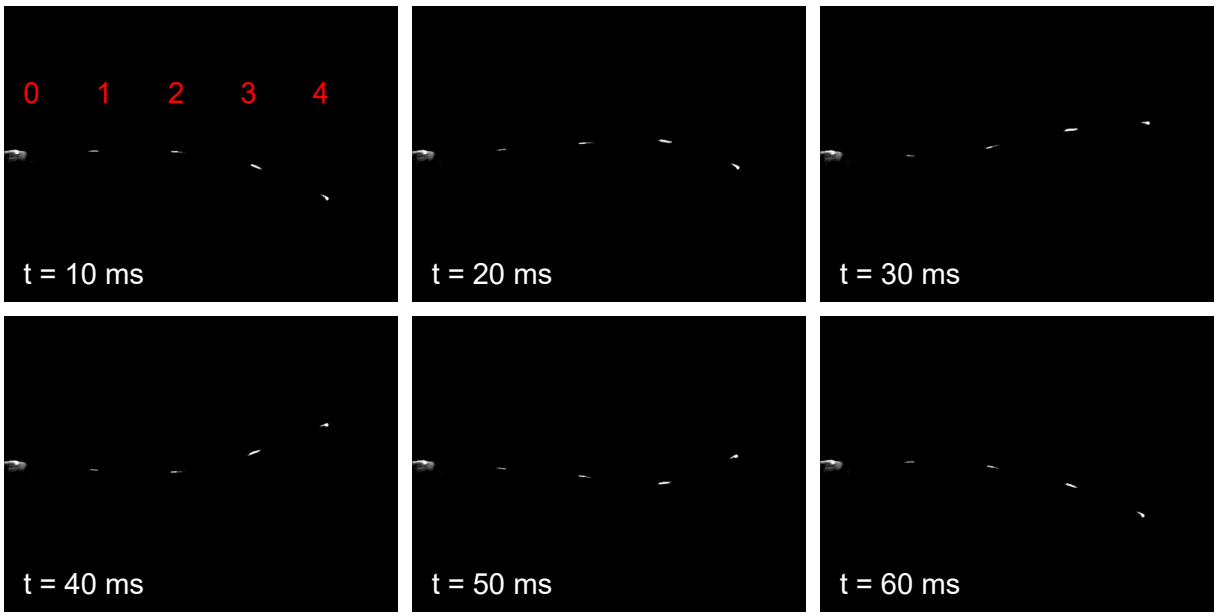

Figure 3. A series of photos at different instants of the substrate fluttering at the air velocity of 3 m/s.

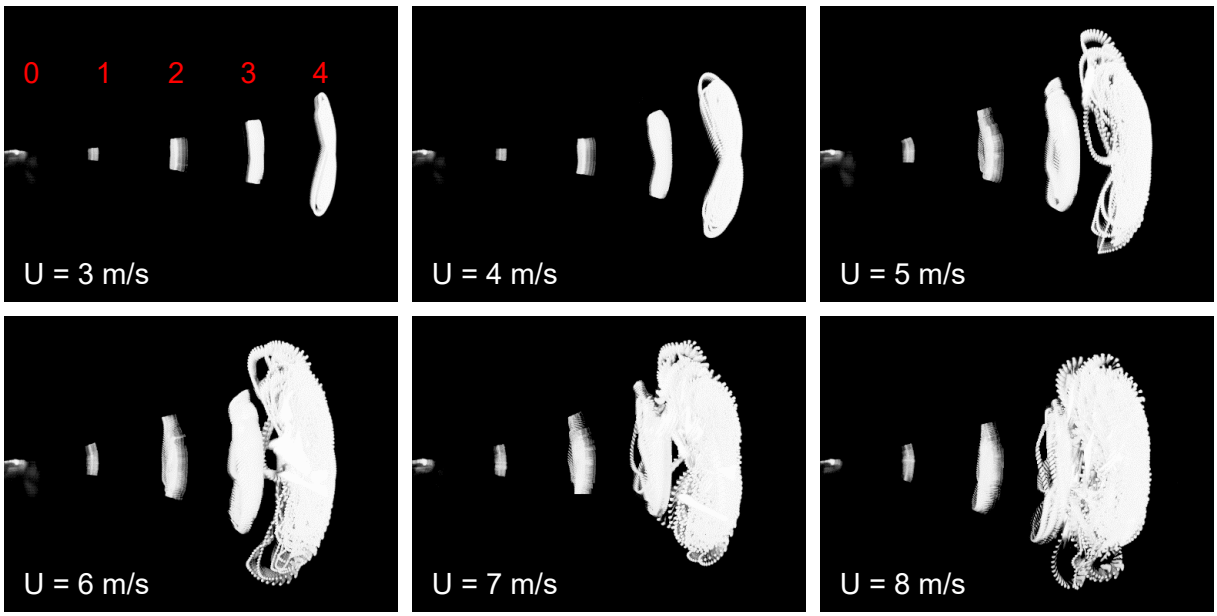

Figure 4. Stacked images of traces within one second of the substrate fluttering at different air velocities *U*.

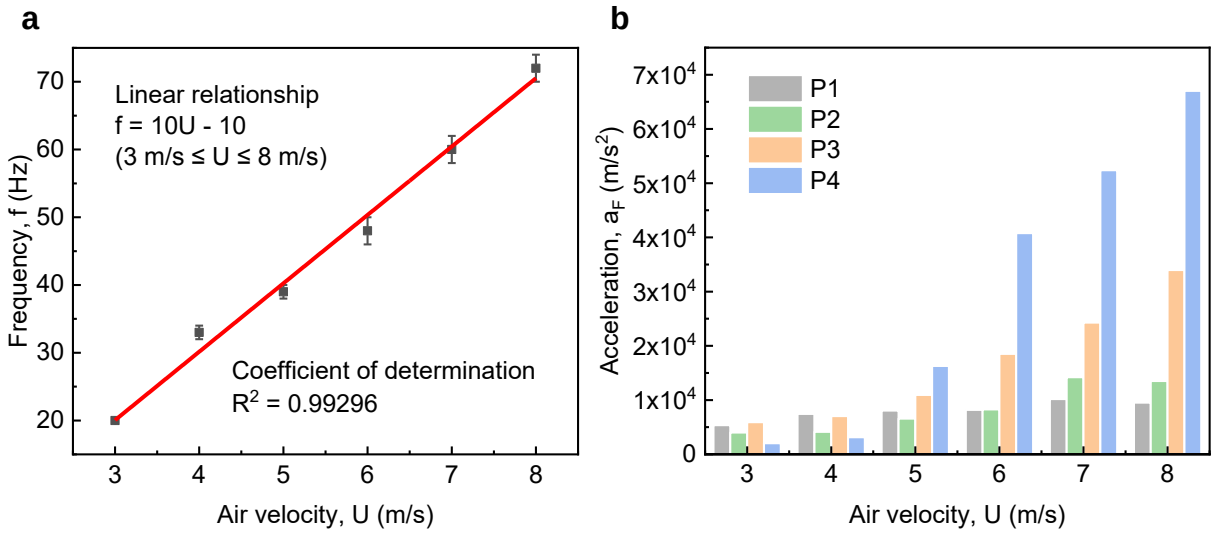

Figure 5. Motion parameters of the fluttering substrate. **a,** Fluttering frequency versus air velocity. All frequency experiments were performed in triplicate, and data are expressed as the mean ± standard deviation. **b,** Fluttering acceleration versus air velocity at different positions. The fluttering acceleration here is the maximum acceleration during experiments, so there are no error bars for it.

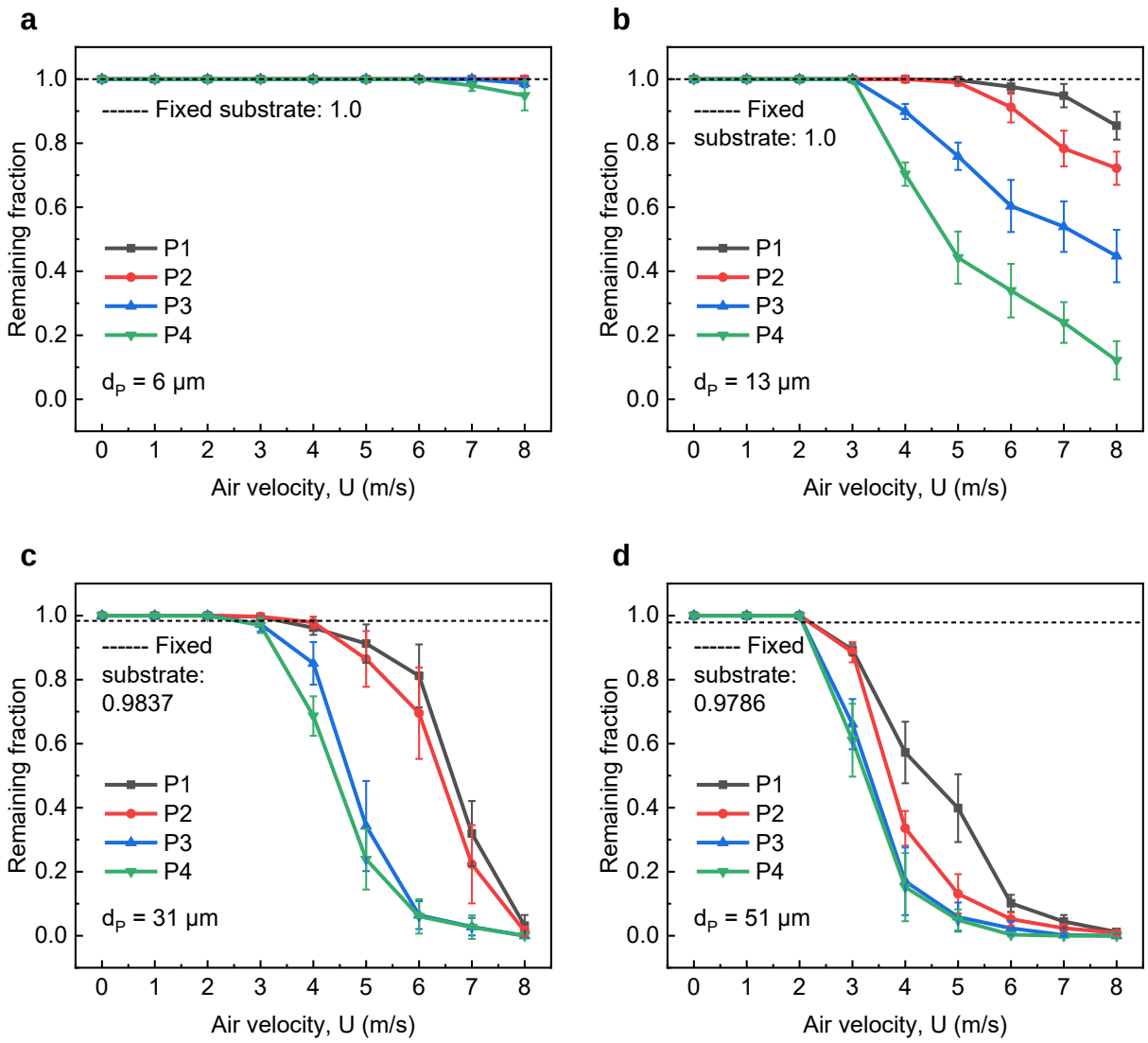

Figure 6. Remaining fraction versus air velocity with respect to different particle diameters. **a,** d_P = 6 µm. **b,** d_P = 13 µm. **c,** d_P = 31 µm. **d,** d_P = 51 µm. All resuspension experiments were performed in triplicate, and data are expressed as the mean ± standard deviation. Dashed lines represent the average results for the fixed substrate case.

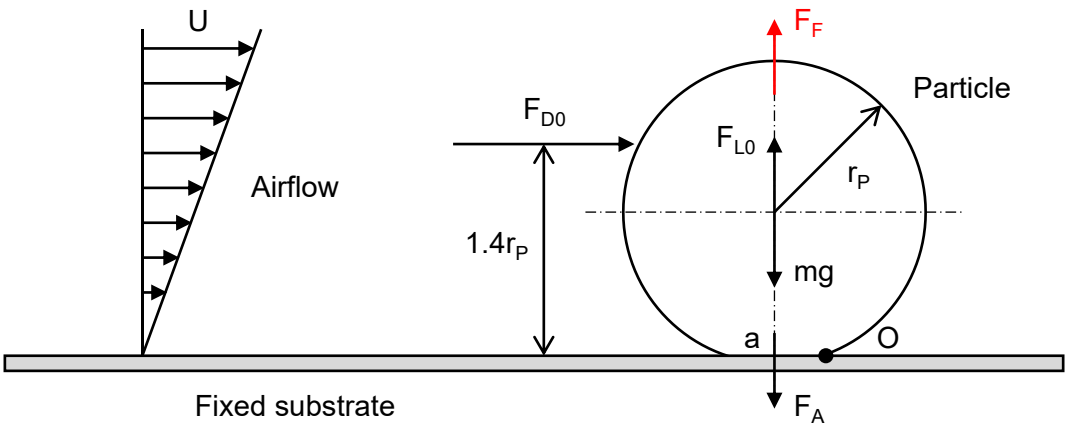

Figure 7. Forces acting on a particle on the substrate under the influence of airflow.

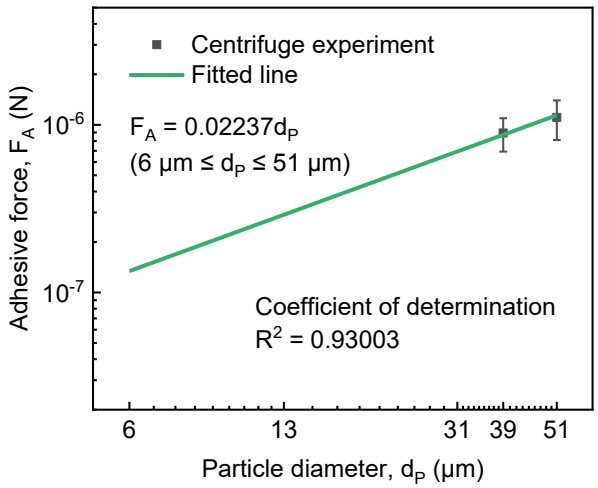

Figure 8. Adhesive force versus particle diameter. All centrifugal experiments were performed in triplicate, and data are expressed as the mean ± standard deviation. This fitted equation is only applicable to the adhesive force prediction in the present work. The adhesive force F_A here is the mean value of adhesive force.

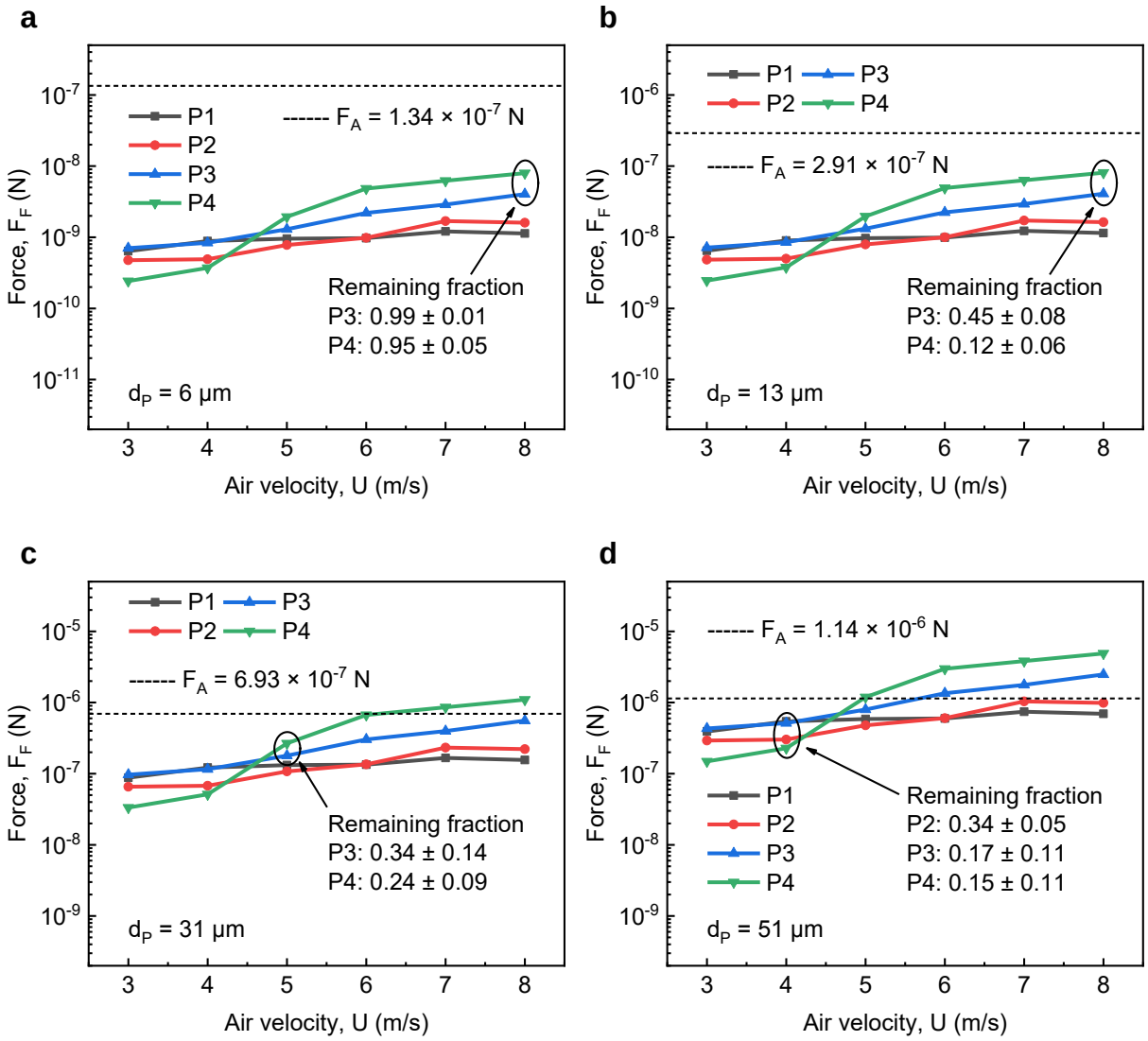

Figure 9. Comparison between the force F_F and the adhesive force F_A with respect to different particle diameters. **a,** d_P = 6 µm. **b,** d_P = 13 µm. **c,** d_P = 31 µm. **d,** d_P = 51 µm. Dashed lines represent the adhesive force F_A.

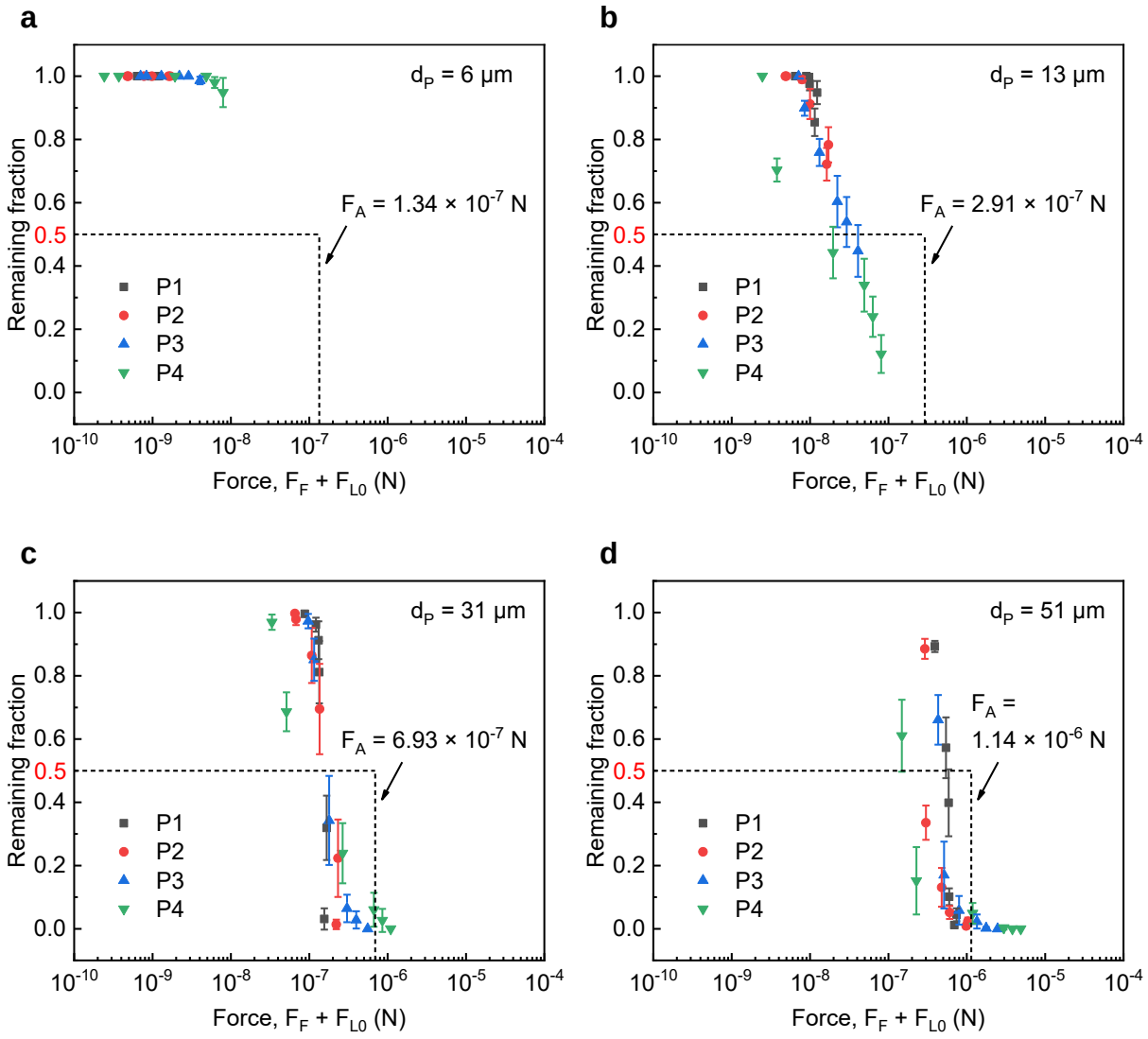

Figure 10. Force analysis for lift-off mode in the fluttering substrate case with respect to different particle diameters. **a,** d_P = 6 μm. **b,** d_P = 13 μm. **c,** d_P = 31 μm. **d,** d_P = 51 μm. All resuspension experiments were performed in triplicate, and data are expressed as the mean ± standard deviation. The horizontal dashed lines represent the remaining fraction of 0.5. The vertical dashed lines represent the adhesive force F_A. The point of intersection (F_A, 0.5) of these two dashed lines represents that the remaining fraction is assumed to be 0.5 at the adhesive force F_A.

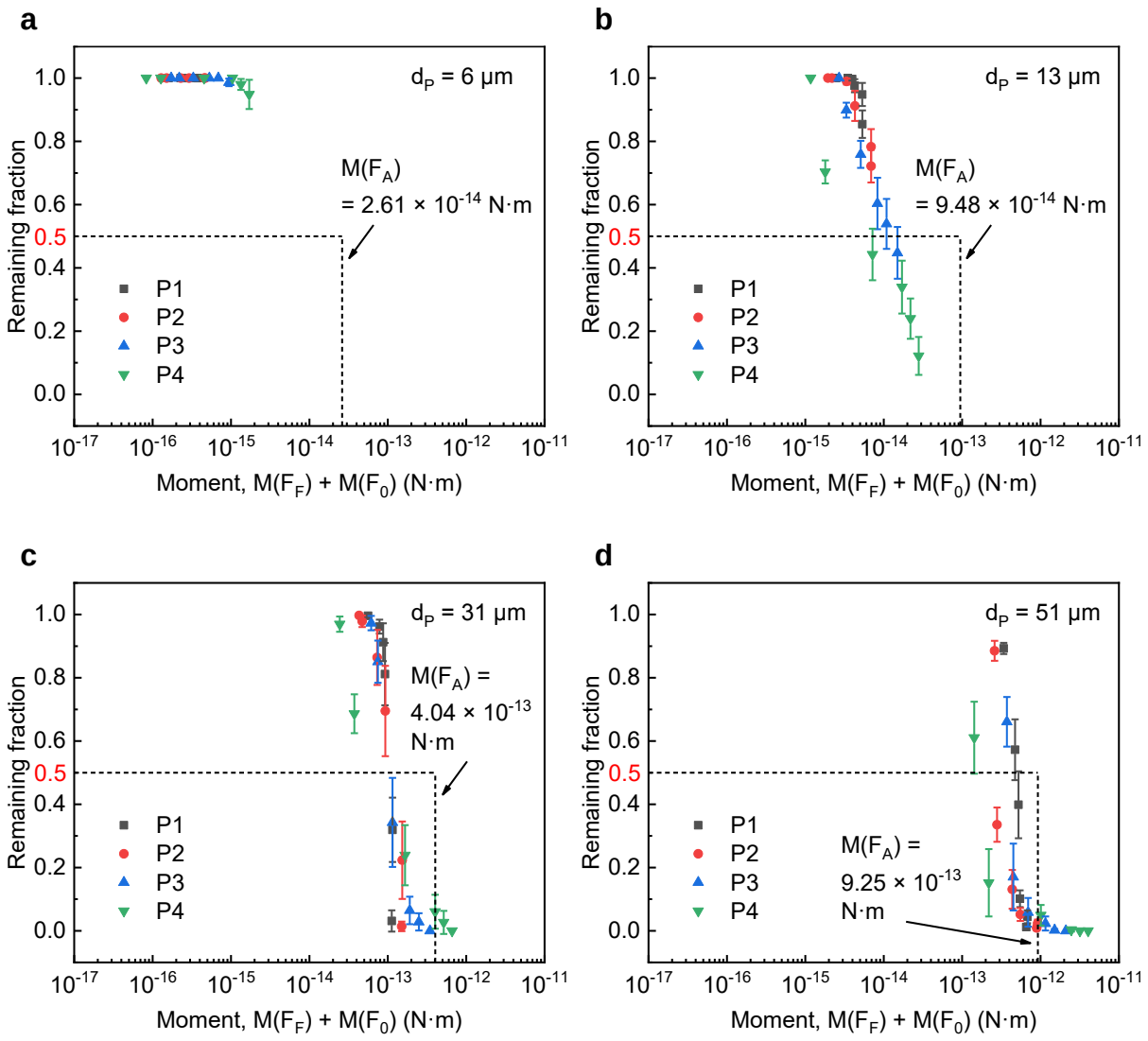

Figure 11. Moment analysis for rolling mode in the fluttering substrate case with respect to different particle diameters. **a,** d_P = 6 μm. **b,** d_P = 13 μm. **c,** d_P = 31 μm. **d,** d_P = 51 μm. All resuspension experiments were performed in triplicate, and data are expressed as the mean ± standard deviation. The horizontal dashed lines represent the remaining fraction of 0.5. The vertical dashed lines represent the adhesive moment $M(F_A)$. The point of intersection ($M(F_A)$, 0.5) of these two dashed lines represents that the remaining fraction is assumed to be 0.5 at the adhesive moment $M(F_A)$. $M(F_0)$ is the aerodynamic moment in the fixed substrate case, i.e., $1.4r_PF_{D0} + aF_{L0}$.